

UC San Diego

UC San Diego Previously Published Works

Title

Degeneration and impaired regeneration of gray matter oligodendrocytes in amyotrophic lateral sclerosis.

Permalink

<https://escholarship.org/uc/item/8wb9d9qf>

Journal

Nature neuroscience, 16(5)

ISSN

1097-6256

Authors

Kang, Shin H
Li, Ying
Fukaya, Masahiro
et al.

Publication Date

2013-05-01

DOI

10.1038/nn.3357

Peer reviewed



Published in final edited form as:

Nat Neurosci. 2013 May ; 16(5): 571–579. doi:10.1038/nn.3357.

Degeneration and impaired regeneration of gray matter oligodendrocytes in amyotrophic lateral sclerosis

Shin H. Kang^{1,*}, Ying Li^{2,*}, Masahiro Fukaya⁴, Ileana Lorenzini^{1,3}, Don W. Cleveland⁵, Lyle W. Ostrow^{2,3}, Jeffrey D. Rothstein^{1,2,3}, and Dwight E. Bergles¹

¹The Solomon H. Snyder Department of Neuroscience, Johns Hopkins University School of Medicine, Baltimore, MD

²The Solomon H. Snyder Department of Neurology, Johns Hopkins University School of Medicine, Baltimore, MD

³Brain Science Institute, Johns Hopkins University School of Medicine, Baltimore, MD

⁴Department of Anatomy, Kitasato University School of Medicine, Sagamihara, Japan

⁵Ludwig Institute, University of California, San Diego

Abstract

Oligodendrocytes associate with axons to establish myelin and provide metabolic support to neurons. In the spinal cord of ALS mice, oligodendrocytes downregulate transporters that transfer glycolytic substrates to neurons and oligodendrocyte progenitors (NG2⁺ cells) exhibit enhanced proliferation and differentiation, although the cause of these changes in oligodendroglia is unknown. Here we report that there is extensive degeneration of gray matter oligodendrocytes in the spinal cord of ALS mice before disease onset. Although new oligodendrocytes were formed, they failed to mature, resulting in progressive demyelination. Oligodendrocyte dysfunction also is prevalent in human ALS, as gray matter demyelination and reactive changes in NG2⁺ cells were observed in motor cortex and spinal cord of ALS patients. Selective removal of mutant SOD1 from oligodendroglia substantially delayed disease onset and prolonged survival in ALS mice, suggesting that ALS-linked genes enhance the vulnerability of motor neurons and accelerate disease by directly impairing the function of oligodendrocytes.

Users may view, print, copy, download and text and data- mine the content in such documents, for the purposes of academic research, subject always to the full Conditions of use: http://www.nature.com/authors/editorial_policies/license.html#terms

Correspondence: Dwight E. Bergles, Ph.D., The Solomon H. Snyder Department of Neuroscience, Johns Hopkins University School of Medicine, 725 N. Wolfe St., WBSB 1001, Baltimore, MD 21205, 410-955-6939; FAX: 410-614-6249, dbergles@jhmi.edu. Jeffrey D. Rothstein, M.D., Ph.D., Brain Science Institute, Johns Hopkins University, School of Medicine, The John G. Rangos Sr. Building, 855 North Wolfe Street; Room 270, 2nd Floor, Baltimore, MD 21205, 410-614-3846; FAX: 410-614-065, jrothstein@jhmi.edu.

*Equal contribution

Author Contributions

S.H.K., Y.L., J.D.R. and D.E.B. designed the experiments. S.H.K. completed the experiments involving NG2⁺ cell proliferation, cell fate analysis of NG2⁺ cells and oligodendrocytes, and immunocytochemical analysis of oligodendrocyte structure (Figs. 1–6, Supplementary Figs. 1–3, 5). Y.L. performed Western blot analysis from *SOD1* (G93A) mice (Supplementary Fig. 7) and human ALS (Supplementary Fig. 8), histological analysis of human tissue (Fig. 7), analysis of ricin injected mice (Supplementary Fig. 4), and analysis of the *SOD1* (G37R) deleted mice (Fig. 8 and Supplementary Fig. 9). M.F. performed the EM and immunogold EM analysis (Fig. 6, Supplementary Fig. 6); I.L. assisted with the ricin injections; D.W.C. provided the *loxSOD1* (G37R) mice; L.W.O. provided assistance with analysis of the human ALS samples. S.H.K., Y.L., J.D.R. and D.E.B. wrote the manuscript.

Competing financial interests

The authors declare that they have no competing financial interests.

Introduction

Amyotrophic lateral sclerosis (ALS) is an adult-onset neurodegenerative disease characterized by progressive muscle weakness and eventual paralysis. Although disease culminates in the degeneration of motor neurons, non-neuronal cells such as astrocytes and microglia have been shown to play critical roles in the pathogenic process of ALS¹⁻⁴. ALS-linked genes such as *Sod1* are expressed in glia as well as motor neurons, and glial cell dysfunction appears to exacerbate injury to motor neurons, as selective removal of mutant SOD1 from subsets of glia slows disease progression^{2, 3}. However, the vulnerability of distinct populations of glial cells to disease-induced stress, and the contribution of these alterations to the pathogenesis of ALS are not well understood.

Degeneration of motor neurons in the spinal cord is associated with reactive changes in surrounding glia that include cellular hypertrophy and enhanced proliferation. In particular, recent studies indicate that the behavior of NG2⁺ glial cells, a distinct, widely distributed class of progenitor cells that have the capacity to differentiate into oligodendrocytes, is dramatically altered in the spinal cord of ALS (*SOD1* (G93A)) mice^{5, 6}. By end stage of disease, NG2⁺ cells exhibit the highest rate of proliferation of any cell type in the spinal cord, and their differentiation into oligodendrocytes is markedly enhanced⁵, suggesting that there may be a progressive dysfunction of oligodendrocytes in ALS.

In addition to their key role in forming myelin, there is emerging evidence that oligodendrocytes provide crucial metabolic support to neurons^{7, 8}. The monocarboxylic acid transporter 1 (MCT1), a transporter that motor neurons depend on for transfer of glycolytic substrates^{9, 10} is expressed predominantly by oligodendrocytes^{9, 11} and downregulated in the motor cortex of ALS patients and the spinal cord of the *SOD1* (G93A) mouse model of ALS⁹. Together, these profound abnormalities in the oligodendrocyte lineage in ALS may impact motor neuron survival; however, the cause of the enhanced proliferation and differentiation of oligodendrocyte progenitors in ALS mice, and the extent of oligodendrocyte abnormalities in human ALS^{12, 13} are uncertain.

Using *in vivo* genetic fate tracing of oligodendrocytes and their progenitors, we discovered that there was extensive, progressive degeneration of oligodendrocytes in the spinal cord of ALS mice, with less than half of the oligodendrocytes produced in first postnatal month surviving by end stage of disease. Mobilization of oligodendrocyte progenitors occurred first in the ventral gray matter, where motor neurons are located, prior to behavioral manifestation of disease; however, newly formed oligodendrocytes in this region exhibited abnormal morphologies and failed to fully differentiate. Dysfunction of gray matter oligodendrocytes also was prevalent in human ALS, as reactive changes in NG2⁺ cells and demyelination were observed in gray matter of the ventral spinal cord and motor cortex of ALS patients. Genetic deletion of mutant human SOD1 (G37R) from NG2⁺ cells and their oligodendrocyte progeny in mice substantially delayed disease onset and prolonged survival, indicating that expression of this ALS-linked gene in the oligodendrocyte lineage accelerates motor neuron degeneration. The progressive loss of gray matter oligodendrocytes, and

failure to restore these crucial cells, may accelerate disease progression in ALS by depriving motor neurons of essential metabolic support.

RESULTS

Enhanced proliferation of NG2⁺ cells in young ALS mice

The progressive loss of motor neurons in *SOD1* (G93A) ALS mice is accompanied by prominent changes in the behavior of NG2⁺ cells⁵. By end stage of disease, their proliferation rate is 20-fold higher than in wild type mice⁵, and they comprise the majority of actively dividing cells in the spinal cord^{5, 6}. However, the cause of the enhanced proliferation of these glial cells in ALS is unknown. To define when and where NG2⁺ cells first exhibit this altered behavior, we examined the spatio-temporal profile of NG2⁺ cell proliferation over the course of disease. Mice were administered BrdU for five days and cumulative BrdU incorporation was measured in lumbar spinal cord (Fig. 1a,b and Supplementary Fig. 1a). In wild type mice, the number of BrdU⁺ NG2⁺ cells declined with age in all regions examined ($P < 0.001$, one-way ANOVA) (Fig. 1c–e), following the developmental decline in generation of oligodendrocytes from these progenitors^{5, 14, 15}. However, in *SOD1* (G93A) mice, NG2⁺ cells sustained high rates of proliferation into adulthood (Fig. 1c–e). Moreover, unlike the uniform decline in proliferation in wild type mice, NG2⁺ cells in *SOD1* (G93A) mice exhibited regional differences in their response. Enhanced proliferation was most prominent in ventral gray matter, where their rate of division was elevated 2.3-fold compared to control mice by P60 ($P < 0.001$, Student's *t*-test), before ALS mice show disease symptoms¹⁶, and 12.9-fold by P95 ($P < 0.0005$), after they exhibit muscle weakness and tremor¹⁷. NG2⁺ cells in ventral white and dorsal gray matter of ALS mice eventually exhibited enhanced proliferation, although it occurred later and the magnitude of increased cell division was lower than in ventral gray matter (Fig. 1c–e). Thus, NG2⁺ cells in *SOD1* (G93A) mice display abnormal behavior in ventral gray matter before behavioral manifestation of disease.

Despite the enhanced generation of NG2⁺ cells in early stages of disease, their density was not significantly altered until end stage (Fig. 1f–h), suggesting that they are continually removed through death or differentiation. To determine the fate of NG2⁺ cells at early stages of disease, genetic lineage tracing was performed using *PDGFR-CreER;Z/EG* mice⁵. After breeding to *SOD1* (G93A) mice, cohorts of NG2⁺ cells were induced to express EGFP by administering 4-hydroxytamoxifen (4HT) at P30 or P60, and the identity of EGFP⁺ cells in lumbar spinal cord was determined 15 – 60 days later (Fig. 2a and Supplementary Fig. 1b,c). In accordance with the regional differences in NG2⁺ cell proliferation, more EGFP⁺ cells were observed in ventral gray matter by P90 in *SOD1* (G93A) mice (Fig. 2b and Supplementary Fig. 1d–f), while the number of EGFP⁺ cells in other areas was not significantly increased relative to controls. However, by end stage, EGFP⁺ cell density in *SOD1* (G93A) mice was higher than controls in all regions examined, with ventral gray matter exhibiting the greatest accumulation of NG2⁺ cell progeny (Supplementary Fig. 1d–f). As the number of EGFP⁺ cells should remain constant if they have an equal probability of dividing or dying, these results suggest that the enhanced proliferation of NG2⁺ cells is not induced solely by accelerated death of these progenitors.

Oligodendrogenesis without oligodendrocyte accumulation

NG2⁺ cells in the spinal cord of end stage *SOD1* (*G93A*) mice not only proliferate more rapidly, but also differentiate more frequently into oligodendrocytes⁵. To determine where and when this increase in oligodendrogenesis occurs, in *PDGFαR-CreER;Z/EG ± SOD1* (*G93A*) mice we followed the appearance of EGFP⁺ cells that were immunoreactive to anti-APC (CC1), a feature of mature oligodendrocytes. when and where this increase in oligodendrogenesis occurs, we followed the appearance of EGFP⁺ cells in *PDGFαR-CreER;Z/EG ± SOD1* (*G93A*) mice that were immunoreactive to anti-APC (CC1), a feature of mature oligodendrocytes. In accordance with the early maturation of myelinated tracts in the spinal cord¹⁸, few oligodendrocytes (EGFP⁺CC1⁺ cells) were generated from P60 P120 in controls (Fig. 2c–h). In contrast, there was a marked increase in newly generated oligodendrocytes in ventral gray matter of ALS mice ($P < 0.001$, one-way ANOVA)(Fig. 2c–f); there were 10.9-fold more EGFP⁺CC1⁺ cells in this region relative to controls 60 days after labeling ($P < 0.0005$, Student's *t*-test) (Fig. 2f).

An increase in EGFP⁺ oligodendrocytes also was observed in ventral white matter at P90 and end stage in ALS mice, although this increase was smaller than in ventral gray matter (Fig. 2g), and there was no significant change in EGFP⁺ oligodendrocytes relative to control in dorsal gray matter (Fig. 2g,h). As the fate of only a small fraction (~ 15%) of NG2⁺ cells was followed in these experiments, the total number of oligodendrocytes generated during this period is expected to be much greater (by ~ 6–7-fold). Despite this profound increase in oligodendrogenesis, the overall density of oligodendrocytes in the spinal cord of *SOD1* (*G93A*) mice at end stage was unchanged relative to controls (Fig. 2i). These results suggest that there must be a concomitant loss of oligodendrocytes with advancing disease.

Degeneration of early-born oligodendrocytes in ALS mice

To determine the extent of oligodendrocyte survival during the course of disease, we performed genetic fate tracing of oligodendrocytes using *PLP-CreER;ROSA26-EYFP ± SOD1* (*G93A*) mice (Fig. 3a,b). Administration of 4HT at P35 resulted in labeling of 15 – 25 % of oligodendrocytes in ventral gray and white matter regions of the spinal cord. Although cre-mediated recombination occurs in some NG2⁺ cells in the brains of *PLP-CreER;ROSA26-EYFP* mice¹⁹, EYFP was not expressed by these progenitors in the spinal cord of either control or *SOD1* (*G93A*) mice (Supplementary Fig. 2), indicating that this approach can be used to track the survival of spinal cord oligodendrocytes *in vivo*. Quantitative analysis of spinal cords sampled at early time points revealed that the number of EYFP⁺ oligodendrocytes increased gradually for the first two weeks after 4HT administration in both control and *SOD1* (*G93A*) mice¹⁹ and initial labeling of these cells was significantly higher in *SOD1* (*G93A*) mice than controls in ventral gray matter (at P35+15), possibly reflecting enhanced activity of the PLP transgene promoter. To allow direct comparison of oligodendrocyte survival between control and ALS mice, the number of EYFP labeled oligodendrocytes in each cohort was normalized to that observed at P35+15, when oligodendrocyte labeling in *SOD1* (*G93A*) mice was near maximum (Fig. 3c,d). In control mice, there was a small increase in EYFP⁺ oligodendrocytes in lumbar spinal cord (EYFP⁺CC1⁺Olig2⁺) 40 and 70 days after initial labeling (at P50) (Fig. 3c), indicating a modest, but continuous labeling of oligodendrocytes during this period. In

contrast, the number of EYFP⁺ oligodendrocytes in *SOD1* (*G93A*) mice was reduced by 22 % 40 days after labeling ($P < 0.05$, one-way ANOVA with Tukey) (Fig. 3c). This loss was progressive, as the number of labeled oligodendrocytes was reduced by 65 % at end stage ($P < 0.0005$, one-way ANOVA) (Fig. 3c,e). Moreover, as expected from the regional difference in NG2⁺ cell proliferation and oligodendrogenesis, loss of early-born oligodendrocytes in ALS mice was most prominent in ventral gray matter (Fig. 3c,d). These results indicate that there is already pronounced degeneration of oligodendrocytes in ventral gray matter near motor neurons when mice first exhibit overt signs of disease.

If oligodendrocytes degenerate in the spinal cord of ALS mice, other indications of cell death should be visible. Indeed, some EGFP expressing oligodendrocytes were immunopositive for activated Caspase-3 in the spinal cord of end stage *MOBP-EGFP;SOD1* (*G93A*) mice (Fig. 4a), in which only mature oligodendrocytes express EGFP (Supplementary Fig. 3). Moreover, dense cell clusters consisting of EGFP⁺ oligodendrocytes surrounded by activated microglial cells were observed at P90 in ventral gray matter (Fig. 4b). In accordance with the death of early born oligodendrocytes observed through genetic fate tracing, similar microglia-oligodendrocyte (EYFP⁺) aggregates were observed in P90 *PLP-CreER;ROSA26-EYFP;SOD1* (*G93A*) mice, in which oligodendrocytes were labeled at P35 (P35+55) (Fig. 4c); however, microglial clustering was not observed near GFAP⁺ astrocytes (Fig. 4c). As microglia are attracted to apoptotic cells²⁰, the presence of these cell aggregates may indicate that mature oligodendrocytes in this region were dying through apoptotic death.

Widespread axonal degeneration can lead to loss of oligodendrocytes and reactive changes in their progenitors^{21, 22}, raising the possibility that degeneration of gray matter oligodendrocytes in ALS mice is secondary to motor neuron degeneration. To address whether loss of motor neurons is sufficient to induce mobilization of NG2⁺ cells, we partially ablated motor neurons by injecting ricin into the sciatic nerve²³. One week after this manipulation, approximately half of the motor neurons in the ventral horn had degenerated on the side ipsilateral to the injection ($P < 0.0005$, paired Student's *t*-test) (Supplementary Fig. 4a–c). However, neither the morphology nor the proliferation rate of NG2⁺ cells, as assessed by NG2 and Ki67 immunoreactivity, respectively, was altered by this loss of motor neurons (Supplementary Fig. 4b,d) suggesting that acute motor neuron death is not sufficient to induce activation and recruitment of these progenitors.

To determine when oligodendrocytes begin to exhibit abnormalities in ALS mice, we examined their morphology in *MOBP-EGFP ± SOD1* (*G93A*) mice at different stages of disease. Oligodendrocyte somata (EGFP⁺Olig2⁺) in the spinal cord of control *MOBP-EGFP* mice had a consistent oval shape (Fig. 5a upper panel and Supplementary Fig. 3). In the spinal cord of end stage *MOBP-EGFP;SOD1* (*G93A*) mice, there was a dramatic increase in irregularly shaped EGFP⁺ structures, many of which were Olig2[−] and lacked nuclei (Fig. 5b lower panel and Supplementary Fig. 5a), reminiscent of the fragmentation that occurs during apoptotic cell death²⁴. Despite this increase in EGFP⁺ structures, the density of EGFP⁺Olig2⁺ oligodendrocytes in end stage *SOD1* (*G93A*) mice was not different from control (Control: 1137 ± 61 cells; *SOD1* (*G93A*): 1233 ± 73 cells, $n = 9$ sections, 3 mice per group, $P = 0.33$, Student's *t*-test), consistent with results obtained using CC1

immunoreactivity (see Fig. 2i). Irregularly shaped EGFP⁺ oligodendrocyte somata with reduced or absent Olig2 immunoreactivity also were observed at earlier stages of disease (Supplementary Fig. 5b,c). To evaluate the progressive nature of these changes, the area of EGFP⁺ cell fragments was measured following digital subtraction of EGFP⁺Olig2⁺ somata (Supplementary Fig. 5d). EGFP⁺ cellular fragments were evident at P90 in *SOD1* (*G93A*) mice, but rarely observed in aged matched controls (volume of fragments: Control: $10 \pm 5.1 \mu\text{m}^3$; *SOD1* (*G93A*): $131 \pm 13 \mu\text{m}^3$, $P < 1.0 \times 10^{-5}$, Student's *t*-test) (Fig. 5c), indicating that pathological alterations in oligodendrocytes are widespread by the time mice begin to show behavioral manifestation of disease.

Myelin deficits in spinal cord gray matter of ALS mice

The accelerated turnover (i.e. death and subsequent regeneration) and abnormal structure of oligodendrocytes in ALS mice, suggests that the state of myelination in gray matter may be altered in disease. Indeed, electron microscopic (EM) analysis of ventral gray matter revealed that the proportion of ultrastructurally normal axons with immature myelin, as evidenced by the presence of a thick layer of oligodendrocyte cytoplasm between the axon and initial myelin wraps, was 49 % higher in end stage *SOD1* (*G93A*) mice compared to age-matched controls (percentage of axons with immature myelin: Control: 9.3 ± 1.2 %; *SOD1* (*G93A*): 13.9 ± 1.0 %, $n = 3$ mice per group, $P < 0.01$, unpaired Student's *t*-test) (Fig. 6a), suggesting that viable, uninjured axons were being remyelinated in ALS mice. Axons with disorganized microtubules, electron dense bodies and spheroids surrounded by swollen, electron dense myelin, typical of Wallerian degeneration¹⁷ also were common in the ventral gray matter of *SOD1* (*G93A*) mice (Supplementary Fig. 6a). Moreover, myelin basic protein (MBP) immunoreactivity was more diffuse in ventral gray matter of *SOD1* (*G93A*) mice at end stage and often not co-localized with EGFP, in contrast to the filamentous EGFP⁺ processes present in control *MOBP-EGFP* mice (Fig. 6b). Axons with mature myelin had thicker myelin sheaths and lower g ratios in *SOD1* (*G93A*) mice compared to controls (Supplementary Fig. 6b–d), possibly reflecting shrinkage of axons from metabolic stress or abnormal patterns of gene expression in oligodendrocytes.

To determine the structure of oligodendrocytes generated after P60, we used membrane anchored EGFP Cre reporter mice *ROSA26-mEGFP* (*mT/mG*) to visualize their fine cellular processes⁵. *PDGF α R-CreER;ROSA26-mEGFP* \pm *SOD1* (*G93A*) mice were injected with 4HT at P60 and analyzed two months later (Fig. 6c). In control mice (P60+60), numerous thin, unbranched EGFP⁺ processes were visible throughout the ventral gray matter, consistent with the morphology of normal internodal segments (Fig. 6d upper panel). Although oligodendrocytes generated after P60 in *SOD1* (*G93A*) mice also were CC1⁺ (see Fig. 2c–e), their processes were highly branched with numerous varicosities (Fig. 6d lower panel); the processes of these newly generated oligodendrocytes often did not co-localize with MBP, in contrast to oligodendrocyte processes in controls (Fig. 6e). Immunogold EM labeling of EGFP revealed that adult-born oligodendrocytes in *SOD1* (*G93A*) mice were frequently associated with degenerating axons (Fig. 6f,g), suggesting that these axons had experienced at least one round of demyelination and remyelination. In addition, there were many irregularly shaped, immunogold-positive structures in *SOD1* (*G93A*) mice that were not associated with axons (Fig. 6h), reminiscent of the oligodendrocyte fragmentation

observed through confocal microscopy (see Fig. 5b). Thus, oligodendrocytes generated in this disease context do not achieve the normal structure of myelinating oligodendrocytes.

Despite the presence of some axons with thicker myelin in *SOD1* (*G93A*) mice, western blot analysis indicated that myelin-associated proteins MBP, CNPase (2', 3',- cyclic nucleotide-3'-phosphodiesterase), and MOG (myelin-oligodendrocyte glycoprotein) progressively decreased with age (Supplementary Fig. 7a,b), with the mature myelin protein MOG exhibiting the earliest decline by P60; this reduction in myelin was most prominent in ventral gray matter (Supplementary Fig. 7c). The decrease in myelin protein expression was accompanied by a concomitant increase in PDGFR α expression in both symptomatic (P90) and end stage mice (Supplementary Fig. 7a,b). Although NG2⁺ cell density in the spinal cord of *SOD1* (*G93A*) mice was not significantly changed at earlier stages of disease (see Fig. 2f–h), the increased expression of PDGFR α from P90 is consistent with progressive mobilization of these progenitors in response to the loss of oligodendrocytes^{25–27}. Together, these findings indicate that myelination is significantly disrupted in the spinal cord ventral gray matter of ALS mice.

Reactive NG2⁺ cells and focal demyelination in ALS

NG2⁺ cells are abundant in the human CNS and are likely to be major contributors to the regeneration of oligodendrocytes in demyelinating diseases such as multiple sclerosis (MS)²⁸. To determine whether NG2⁺ cells also undergo reactive changes in ALS patients, immunohistochemistry was performed on human motor cortices. Motor cortex was analyzed rather than spinal cord, as this tissue is better preserved in human autopsies, which is required to preserve the NG2 proteoglycan. Sections also were immunostained for the microglial antigen Iba1 to distinguish NG2⁺ glial cells from NG2 expressing macrophages/microglia that often appear in chronic disease and CNS injury^{29, 30}. NG2 immunoreactivity was markedly higher in the motor cortex of ALS patients, compared to either motor cortex from non-ALS subjects (Control: 106.2 ± 5.3 %; ALS: 200.2 ± 9.4 %, $P < 0.0001$, unpaired Student's *t*-test) or occipital cortex from the same patients, as determined by the intensity of NG2-immunoreactivity (Fig. 7a; Supplementary Fig. 8a,b). Although NG2⁺Iba1⁺ cells were observed in both control and ALS motor cortex, thicker NG2⁺ processes that exhibited signs of hypertrophy in ALS tissue were Iba1[−] (Supplementary Fig. 8a), indicating that NG2⁺ glial cells exhibit reactive changes in regions of brain where motor neurons degenerate in ALS.

To assess whether these changes in NG2⁺ cells also were associated with degeneration of oligodendrocytes in gray matter, we examined the integrity of myelin in motor cortex and spinal cord of sporadic and familial ALS patients. Myelin staining (Luxol fast blue) and MBP immunolabeling revealed areas of focal loss of myelin in motor cortex gray matter of ALS patients that were not observed in control patients (Fig. 7b,c) (see Supplementary Table 1). Moreover, in addition to the well-described reduction in myelination of corticospinal tracts, myelin was also reduced in ventral horn gray matter of the spinal cord from ALS patients (Fig. 7d). To quantify the extent of myelin loss, MBP and CNPase abundance was determined in randomly sampled regions of primary motor cortex gray matter (Fig. 7e,f and Supplementary Fig. 8c,d), as well as spinal cord ventral gray matter (Fig. 7g,h). MBP

expression was significantly lower in most ALS patients relative to controls, while CNPase levels were significantly reduced in one patient and trended lower in a second patient. Furthermore, the reduction in expression of myelin proteins was greater in motor cortices as compared to occipital cortices in the same ALS patients, consistent with motor cortex specific lesions (Supplementary Fig. 8c,d). Although it is not yet possible to determine the relative contributions of primary oligodendrocyte death and secondary oligodendrocyte death due to Wallerian degeneration in these tissues, these results indicate that demyelination of gray matter regions where motor neurons are located is a common feature of human ALS.

Mutant SOD1 deletion from oligodendroglia reduces disease

Oligodendrocytes are vulnerable to damage through cell-autonomous expression of genes linked to neurodegeneration^{31, 32}, particularly aggregation-prone proteins, raising the possibility that expression of mutant SOD1 in oligodendrocytes may impair their function and promote motor neuron degeneration. To determine if there is an oligodendroglial contribution to disease in ALS, we selectively removed mutant human SOD1 (G37R) from NG2⁺ cells in *PDGFαR-CreER;loxSOD1(G37R)* mice². Administration of 4HT to these animals at P18 and P30 to selectively remove significantly decreased *SOD1 (G37R)* gene level in NG2⁺ cells by ~ 43 % as determined by qPCR (Fig. 8d), but preserved its expression in motor neurons (Supplementary Fig. 11a); this approach had little impact on overall tissue levels of SOD1 (G37R) (Supplementary Fig. 11b,c), in keeping with the relatively small number of NG2⁺ cells present (2–5 % of all neural cells in the spinal cord)³³. However, selective removal of SOD1 (G37R) from oligodendroglia profoundly delayed disease onset by 69 days (median, $P = 0.0002$), delayed early disease by 83 days (median, $P = 0.0002$), and prolonged survival by more than 130 days (median, $P < 0.005$) (Fig. 8a,b). Consistent with this delay in disease, these mice exhibited less astrogliosis and microglial activation in the spinal cord (Supplementary Fig. 9d). The time from symptom onset to death (e.g. disease duration) was not altered by removal of SOD1 (G37R) from oligodendroglia (–4HT: 180 ± 17 d; +4HT: 209 ± 15 d, mean \pm s.e.m.; $n = 12$ mice per group, $P = 0.246$, Mann Whitney test), indicating that the prolonged survival of these animals resulted primarily from a delay in disease onset. This manipulation decreased *SOD1 (G37R)* gene level in NG2⁺ cells by ~ 43 %, as determined by qPCR from isolated NG2⁺ cells (data not shown), but preserved its expression in motor neurons (Supplementary Fig. 9a). Although this approach had little impact on overall tissue levels of SOD1 (G37R) (Supplementary Fig. 9b,c), in keeping with the relatively small number of NG2⁺ cells present (2–5 % of all neural cells in the spinal cord)³³, it presumably affected all oligodendrocytes generated from *SOD1 (G37R)* deleted-NG2⁺ cells.

Previous studies indicate that oligodendrocytes present at end stage of disease in *SOD1 (G93A)* mice express much less MCT1⁹. As oligodendrocytes provide metabolic support to axons via this transporter and its expression is downregulated in *SOD1 (G93A)* mice⁹, we evaluated MCT1 expression in SOD1 (G37R) deleted mice. Removal of SOD1 (G37R) from oligodendroglia helped preserve MCT1 expression in some animals at early stages of disease (Fig. 8c). Together, these data indicate that expression of mutant SOD1 in NG2⁺ cells and their oligodendrocyte progeny has a deleterious effect on motor neuron survival,

and suggest that one negative consequence of mutant SOD1 expression in oligodendrocytes is to diminish their capacity to provide metabolic support to neurons.

Discussion

Oligodendrocytes form myelin sheaths around axons in the CNS that enable rapid conduction of action potentials at minimal energetic cost. However, the perception that oligodendrocytes are primarily structural elements has been challenged by recent evidence that they also provide metabolic support to neurons by transferring glycolytic intermediates³⁴ through the monocarboxylic transporter MCT1⁹. Motor neurons in the spinal cord depend on this transporter for survival, suggesting that oligodendrocyte integrity impacts motor neuron fate. Here, we report that there is extensive degeneration of gray matter oligodendrocytes in ALS mice that begins prior to the onset of behavioral symptoms of disease. Although NG2⁺ progenitor cells are mobilized to regenerate oligodendrocytes, oligodendrocytes generated in later stages of disease exhibit aberrant morphologies and fail to restore myelin (*see* Supplementary Fig. 10). A reduction in gray matter myelin and reactive changes in NG2⁺ cells were frequently observed in the motor cortex and spinal cord of ALS patients, indicating that degeneration of gray matter oligodendrocytes is prevalent in human ALS. Selective deletion of mutant SOD1 protein from oligodendroglia delayed disease onset and prolonged survival in mice, pointing to a key role for these cells in the precipitation of disease in ALS. Together, these results suggest that the profound loss of gray matter oligodendrocytes in ALS, and the inability to restore oligodendrocyte function, accelerates injury to vulnerable motor neurons.

There is accumulating evidence that ALS is not strictly a disease of motor neurons^{1–3, 35, 36}. Selective removal of mutant SOD1 (G37R) from motor neurons slowed disease onset, but did not alter disease progression, indicating that expression of this mutant gene in other cell types is sufficient to cause motor neuron death². In particular, astrocytes appear to be important contributors to disease, as there is a dramatic reduction in astrocyte glutamate transporter expression in mouse models of ALS³⁵ and ALS patients³⁷, astrocytes from *SOD1* (G93A) mice secrete factors that are toxic to motor neurons³⁸, and removal of mutant SOD1 from astrocytes delays microglial activation and extends animal survival³. However, expression of mutant SOD1 only in astrocytes is not sufficient to induce disease³⁹, indicating that astrocyte dysfunction combines with other cellular alterations to accelerate the death of motor neurons.

The consequences of mutant protein expression in oligodendrocytes has been examined using chimeric mice, in which oligodendrocytes and motor neurons expressed mutant SOD1, while all other cells expressed either wild type or mutant SOD1⁴⁰. Remarkably, most of these mice survived significantly longer than mice that expressed SOD1 (G37R) ubiquitously, and did not exhibit motor neuron degeneration at the time of sacrifice, suggesting that alterations in cells other than motor neurons and oligodendrocytes are critical for determining disease onset. Nevertheless, our results indicate that selective removal of this mutant protein from oligodendrocyte progenitors profoundly slows disease progression. It is possible that ALS-linked gene mutations render oligodendrocytes more vulnerable to stresses created by abnormalities in other cells, and that oligodendrocyte

degeneration is a critical common pathway that forces motor neuron degeneration. Indeed, oligodendrocyte vulnerability may be exacerbated by the presence of pro-inflammatory cytokines such as interferon- γ ⁴¹, which at high levels induces apoptosis of oligodendrocytes⁴². Expression of mutant SOD1 in oligodendrocyte progenitors also may induce long-term changes in gene expression that increase the vulnerability of oligodendrocytes.

Mutations in genes linked to ALS, such as *Sod1* (SOD1), *Tardbp* (TDP-43), and *Fus* (FUS), cause the formation of protein aggregates, often leading to endoplasmic reticulum (ER) stress that can induce apoptosis. Ubiquitinated protein aggregates containing TDP-43 have been observed in oligodendrocytes in patients with frontotemporal lobar degeneration (FTLD)⁴³, and other mutant proteins, such as α -synuclein⁴⁴ and tau⁴⁵ accumulate in oligodendrocytes in patients with multiple system atrophy (MSA) and other types of frontotemporal dementia. These observations raise the possibility that expression of aggregation-prone mutant proteins in oligodendrocytes compromises their ability to provide adequate support to neurons. Indeed, selective overexpression in oligodendrocytes of a mutant form of tau (P301L) associated with human FTD (FTDP-17) led to formation of filamentous tau⁺ inclusions in these cells, eventual oligodendrocyte degeneration and reduced myelin³¹. These animals also exhibited impaired axonal transport, muscle atrophy and hind limb weakness, suggestive of motor neuron degeneration. We observed that oligodendrocyte degeneration in the spinal cord of ALS mice and demyelination in the brains of ALS patients were prominent in gray matter regions near motor neurons, indicating that oligodendrocytes in these regions are more susceptible to disease-related stresses. Indeed, previous studies have shown that oligodendrocytes in the spinal cord gray matter are particularly vulnerable to ER stress when proteolipid protein (PLP), a component of myelin, is overexpressed⁴⁶. Thus, the regional bias in oligodendrocyte vulnerability may depend more on metabolic demand, which is related to the type of associated neuron, rather than the need for myelination.

Although oligodendrocyte degeneration may be a secondary consequence of motor neuron death in ALS, motor axons represent only a minor portion of myelinated fibers in spinal cord gray matter. As each oligodendrocyte in the spinal cord forms on average ~ 25 internodal segments⁴⁷, each with a different axon, it seems likely that there would be sufficient remaining axons to promote oligodendrocyte survival, unless dying motor neurons produce pro-apoptotic signals. Furthermore, enhancing oligodendrogenesis without appropriate target axons to myelinate would appear maladaptive. Indeed, the increase in ultrastructurally normal axons with immature myelin sheaths in ventral gray matter of end stage *SOD1* (G93A) mice (see Fig. 6a), suggests that oligodendrocytes are attempting to remyelinate viable axons, rather than simply degenerating as a result of axon loss. Our results also indicate that selective degeneration of motor neurons is not sufficient to enhance the proliferation of NG2⁺ cells in the spinal cord (see Supplementary Fig. 4), which is expected to occur if new oligodendrocytes are being formed^{17, 23, 24}. Conversely, degeneration of oligodendrocytes and demyelination are sufficient to induce neuronal apoptosis, as seen after genetically induced oligodendrocyte ablation^{25, 26} and in multiple

sclerosis (MS)⁴⁸. Therefore, oligodendrocyte loss is expected to have a profound negative impact on the integrity and survival motor neurons during the course of disease.

When do oligodendrocytes begin to degenerate in ALS? Although proliferation of NG2⁺ cells was enhanced well before behavioral onset of disease, their density did not increase, due to a concomitant increase in the proportion of cells undergoing differentiation. If this increase in oligodendrogenesis compensates for cells lost or injured, as expected from the maintenance of oligodendrocyte number (*see* Fig. 2), then oligodendrocyte degeneration is a very early event in the disease process. Despite the continuous regeneration of oligodendrocytes, the proportion of incompletely myelinated axons increased, myelin levels were reduced, and oligodendrocytes failed to express MCT1, indicating that their maturation was impaired. In addition, adult-born oligodendrocytes exhibited morphological characteristics of apoptosis, suggesting that their turnover is accelerated. This expanding cycle of proliferation, differentiation, and death in the oligodendrocyte lineage in ALS may accelerate damage to vulnerable motor neurons by consuming resources and triggering reactive changes in other glial cells (*see* Supplementary Fig. 10).

The degeneration of oligodendrocytes and impaired maturation of oligodendrocyte progenitors in ALS shares similarities to progressive forms of MS, where impaired remyelination following immune-mediated attack of oligodendrocytes leads to neuronal degeneration. Indeed, there is increasing appreciation of gray matter demyelination in MS⁴⁹. Thus, therapeutic approaches that are being developed to treat MS, based on promotion of oligodendrocyte survival or enhancement of oligodendroglial metabolic support to neurons, also may be helpful for preventing motor neuron degeneration in ALS.

Methods

Animals

*PDGFaR-CreER*⁵ and *loxSOD1 (G37R)*² mice were generated and described previously. *PLP-CreER*⁵⁰ Tg mice were kindly provided by Dr. Brian Popko (U Chicago). *SOD1 (G93A)*, *ZEG*⁵¹, *ROSA26-EYFP*⁵² and *ROSA26-mEGFP (mT/mG)*⁵³ mice were purchased from the Jackson Laboratory. *MOBP-EGFP* mice were generated by GENSAT⁵⁴ and purchased from the Mutant Mouse Regional Resource Center (MMRRC). All experiments were carried out in strict accordance with protocols approved by the Animal Care and Use Committee at Johns Hopkins University.

BrdU labeling and Cre activity induction

For continuous exposure to BrdU (Sigma), mice were provided with BrdU-containing drinking water (1 mg/ml supplemented with 1 % sucrose), and received additional BrdU injections twice a day (50 mg/kg, i.p., at least 8 hours apart) for 5 consecutive days. 4-hydroxytamoxifen (4HT, Sigma H7904) was administered, 2 mg (to *PLP-CreER;ROSA26-EYFP*) or 4 to 5 mg (to *PDGFaR-CreER;ZEG* or *PDGFaR-CreER;mTmG*) by i.p. injection either at P30 or P60. For the excision of *SOD1 (G37R)*, 4HT was injected to *PDGFaR-CreER; loxSOD1 (G37R)* mice at P18 (1 mg) and at P30~P31 (total 4 mg). Each mouse received up to two injections per day (1 mg per injection), at least 8 hours apart.

Ricin injection

After anesthesia to P20 mice with Ketamine (120 mg/kg) and Xylazine (8 mg/kg, i.p.), the sciatic nerve was exposed and crushed with a fine forcep for 20 seconds, followed by 1 μ l of 1mg/ml ricin (Sigma) injection into the nerve in the proximal side of the crush, and 1 μ l of PBS in the other side. The animals were sacrificed one week later.

Immunohistochemistry

Mice were deeply anesthetized with sodium pentobarbital (100 mg/kg b.w.) and perfused transcardially with 4 % paraformaldehyde (PFA in 0.1M phosphate buffer, pH 7.4). Spinal cords were further post-fixed overnight at 4 °C. For immunofluorescence, lumbar spinal cords were stored at 4 °C for more than 36 hours in 30 % sucrose solution (in PBS, pH 7.4), and then sectioned with a cryostat (35 μ m or 25 μ m thick). Immunofluorescence was performed on free-floating sections as described previously⁵. We used primary antibodies to APC (CC1) (mouse, Calbiochem, 1:50), BrdU (rat, Accurate, 1:500), Caspase-3 (rabbit, Cell Signaling, 1:500), ChAT (goat, Millipore, 1:300), EGFP (goat, Frontier Institute, 1:500), EGFP (rabbit, a gift from Dr. Richard Haganir, Johns Hopkins University, 1:500), GFAP (mouse, NeuroMab, 1:500), GFAP (rabbit, DAKO, 1:1,000), Iba1 (rabbit, Wako, 1:1,000), Ki67 (rabbit, Abcam, 1:500), NG2 (guinea pig, 1:3,600), Olig2 (guinea pig, a gift from Dr. Ben Novitsch, UCLA, 1:20,000), Olig2 (rabbit, Millipore, 1:500), PDGFR (rabbit, a gift from Dr. William Stallcup, Burnham Institute, 1:500), SMI32 (mouse, Covance, 1:1,000), and hSOD1 (rabbit, 1:70). Secondary antibodies were Alexar Fluor 488-(Invitrogen 1:500), or Cy3-, DyLight 549-, Cy5-, or DyLight 649- conjugated donkey F(ab')₂ fragments against rabbit, goat, mouse, rat, or guinea pig (Jackson ImmunoResearch). For Olig2, ALDH or APC (CC1) immunostaining, tissue sections were incubated in LAB solution (Polysciences) for 10 minutes before blocking. For BrdU staining, sections were preincubated in 2N HCl at 37 °C for 30 minutes, followed by neutralization with 0.1 M sodium borate buffer (pH 8.5) prior to immunolabeling. DAPI was added during the secondary antibody incubation for most cases. Sections were mounted on slides with ProLong antifade reagent (Invitrogen).

For human tissue histopathological analysis, paraffin-embedded and fresh frozen human primary motor cortex and lumbar spinal cord sections (all 5 μ m thick) were used. Sections were deparaffinized in a series of xylene, 100 % alcohol, 95 % alcohol, 70 % alcohol and water, followed by antigen retrieval (boiling in 10 mM Citrate buffer at pH 6.0 for 10 min). Sections were incubated with 3 % H₂O₂, blocked with 3% BSA in PBS, and incubated with the primary antibody for 60 minutes at room temperature or at 4° C overnight. We used primary antibodies to Iba1 (rabbit, Wako, 1:1,000), MBP (rabbit, Millipore, 1:200), and NG2 (mouse, BD Science, 1:1,000). Sections were incubated with biotinylated secondary antibodies (Vector Lab), followed by VECTASTAIN Elite ABC reagent according to the manufacture's instruction (Vector Lab) and colorimetrically developed using the 3,3'-diaminobenzidine (DAB) substrate kit (Vector Lab). For double labeling of NG2 and Iba1, mounted fresh frozen sections (5 μ m) were fixed with 4 % PFA at room temperature for 15 minutes, incubated with 3 % H₂O₂, blocked with 3 % BSA, and then incubated with anti-NG2 antibody at 4° C overnight. Sections were incubated with HRP labeled secondary antibody and Renaissance TSA Biotin system (PerkinElmer) according to manufacturer's instructions, and developed with DAB substrate. For Iba1 staining, sections was blocked

with the BLOXALL solution (Vector Lab), followed by alkaline phosphatase conjugated secondary antibody (Promega) and developed with NBT/BCIP substrate (Vector Lab).

Luxol fast blue myelin staining

Tissue sections were stained with 0.1 % luxol fast blue solution (Sigma) at 60° C overnight. Sections were rinse with 95 % ethanol and water, reacted with 1 % lithium carbonate solution and 70 % ethanol, followed by rinsing in water. Counter staining with hematoxylin and eosin was performed, as necessary.

Microscopy and cell counting

Mounted slides were imaged using an epifluorescence microscope (Zeiss Axio-imager M1), and Axiovision software (Zeiss), or a confocal laser scanning microscope (Zeiss LSM 510 Meta) using appropriate excitation and emission filters. A total of 3 – 5 sections were examined per mouse, and 3 – 4 mice were analyzed per each data point. Confocal images represent projected stacks of 15 – 45 images collected at 0.5 – 1.5µm steps.

Volume measurement of oligodendrocyte cellular fragments

EGFP⁺ elements of *MOBP-EGFP* mice that are not associated with Olig2 were quantified using a commercially available 3D analysis package (Imaris; Bitplane). EGFP⁺ structures were defined by applying an absolute intensity threshold, followed by thresholding for structure size to remove small objects. Identical thresholds were applied to all images. EGFP⁺ structures that were also associated with Olig2 staining were deleted, as were structures which were positioned at the edge of the imaged field. The volume of Olig2⁻ EGFP⁺ was scaled according to total imaged volume.

Electron microscopy

Mice were perfused transcardially with 4 % paraformaldehyde/2.5 % glutaraldehyde in 0.1 M Phosphate buffer (PB) under deep anesthesia, and brain tissue was isolated and post-fixed for 4 hours at 4 °C. Brains were treated with 2 % OsO₄ for 1 hour, and washed in water. Samples were incubated in 2 % uranyl acetate for 30 minutes and dehydrated using 50 %, 70 %, 90 %, 100 % ethanol, and propylene oxide. Samples were embedded in Epon 812 resin (Ted Pella). Ultrathin sections were obtained using Ultracut UCT (Leica) and stained with 2 % uranyl acetate and lead citrate. Electron micrographs were taken with an H-7600 electron microscope (Hitachi, Tokyo, Japan). Image J was used to measure the diameter of axons and myelin sheath.

For pre-embedding immunoelectron microscopy, 4HT-injected *PDGFaR-CreER;ROSA26-mEGFP ± SOD1 (G93A)* mice (P60+60) were perfused transcardially with 4 % paraformaldehyde/0.1 % glutaraldehyde in 0.1 M PB under deep anesthesia. After blocking with 5% normal donkey serum in PBS, spinal cord sections (50 µm thick) were incubated overnight with rabbit anti-EGFP IgG and then with anti-rabbit IgG conjugated to 1.4 nm gold particles (Nanoprobes). Following silver enhancement (HQ silver, Nanoprobes), sections were osmificated, dehydrated and embedded in Epon 812 resin. Ultrathin sections were prepared with an ultramicrotome (Leica) and stained with 2 % uranyl acetate.

Clinical materials

Human autopsy materials including frozen and paraffin-embedded control and ALS patient cortex and spinal cord tissues were obtained from the Johns Hopkins University ALS Clinic, Brain Resource Center/Department of Pathology, VA Biorepository Brain Bank. All experiments were performed using motor cortex, cervical and/or lumbar spinal cord tissues. All available demographic information for the ALS and control cases analyzed in this study is presented in the Supplementary Table 1.

Western blotting

Lumbar spinal cords were collected from control and *SOD1* (*G93A*) mice, snap frozen in liquid nitrogen, and then stored at -80°C until use. For human cortex protein analysis, the gray matter and white matter were separated grossly. The tissues were homogenized in RIPA buffer (Thermo) supplemented with proteinase inhibitor (Roche) and phosphatase inhibitor (Calbiochem) on dry ice. Thirty microgram of protein was separated on 4 – 12 % gradient Bis-Tris gels (BioRad) or NuPage and transferred to nitrocellulose membranes (BioRad). After blocking with 5 % nonfat milk, membranes were probed with primary antibodies at 4°C overnight, following by HRP conjugated secondary antibodies, Supersignal Pico detection reagent (Pierce), and then exposed to HyBlot CL autoradiography film (Denville). The intensity for each band was quantified with Image J software. The antibodies used for western are antibodies to CNPase (mouse, Millipore, 1:1,000), MBP (mouse, Millipore, 1:2,000), PDGF α R (rabbit, Santa Cruz, 1:200), GAPDH (rabbit, Cell Signaling, 1:1,000) and MCT1 (rabbit, Santa Cruz, 1:100).

Analysis of disease progression

For *PDGF α R-CreER;loxSOD1* (*G37R*) mice, the time of disease onset, early disease and end stage were defined as the time when mouse body weight reached the peak, body weight declined to 10 % of the maximum weight, and paralyzed animals could not right itself within 20 seconds when placed on its side respectively, as previously described². The total disease duration was defined as the duration between disease onset and end stage. Animals were weighted once a week when they were 150 days old.

qPCR determination of transgene excision in NG2⁺ cells

The brain neural cells from two-month old animals (with and without 4HT injection, $n = 3$ each group) were dissociated using Dissociation Kit (P) (Milteny) by following the manufacturer's instructions. Myelin was removed by using Percoll generated gradient. Live cell fraction was collected and the cells were submitted to staining for PDGF α R (1:200, Santa Cruz) and followed by Alexa anti-rabbit 488 before Fluorescence-activated cell sorting (FACS) analysis. Dead cells were excluded by propidium iodide (PI) staining during sorting using MoFlo MLS high-speed cell sorter (Beckman Coulter) at Johns Hopkins School of Public Health FACS core. Only PDGF α R⁺ and PI⁻ cells were sorted out for transgene evaluation. Genomic DNA was extracted by using QIAmp DNA micro kit (Qiagen) following the manufacturer's instructions. qPCR for *SOD1* (*G37R*) transgene was performed using the primers and cycler parameters on ABI Plusone cycler as described previously².

Statistical analysis

All data are presented as mean \pm standard error of the mean (s.e.m.). For multiple groups, data were evaluated by one-way ANOVA and further evaluated with Tukey post hoc comparisons. Otherwise, unpaired Student's *t*-test was applied. *P* < 0.05 was considered to be statistically significant. The paired Student's *t*-test was used to evaluate contralateral and ipsilateral side of cell counts in ricin injected animal study. Log-Rank test was used for survival curve analysis. Mann Whitney test was used for disease duration.

Supplementary Material

Refer to Web version on PubMed Central for supplementary material.

Acknowledgments

We thank Naiqing Ye, Isha Srivastava, Sujal Singh and Truong Le for their excellent technical support, Dr. Michele Pucak for help with Imaris software operation and quantitative analysis, Dr. Jessica Carmen for her contributions to the Cre/lox animal study, and Hao Zhang at the Johns Hopkins University School of Public Health FACS core for assistance with NG2⁺ cell isolation. We thank Dr. Bruce Trapp (Cleveland Clinic Lerner Research Institute) for advice regarding human NG2⁺ cell staining, Dr. Ranjan Dutta (Cleveland Clinic Lerner Research Institute) for advice regarding protein extraction from human tissues, and Dr. Brian Popko (University of Chicago) for providing *PLP-CreER* mice. Human samples were provided by Dr. Robert Bowser at Barrow Neurological Institute, Dr. Katrina Trevor at SACTL-VA Biorepository Trust and SACTL-VA Biorepository Trust, Dr. Thomas Hyde at the Lieber Institute for Brain Development, and the Johns Hopkins School of Medicine Dept. of Neuropathology. We thank Elizabeth Mosmiller for helping with patient demographic information. We also thank Drs. Amit Agarwal and Abraham Langseth for critical discussions. This work was supported by grants from P²ALS (to D.E.B. and J.D.R.), the NIH (NS27036 to D.W.C, NS33958 to J.D.R and NS051509 to D.E.B), the ALS Association (4ZMUDE to Y.L.), the Robert Packard Center for ALS Research at Johns Hopkins, and the Brain Science Institute.

References

1. Clement AM, et al. Wild-type nonneuronal cells extend survival of SOD1 mutant motor neurons in ALS mice. *Science*. 2003; 302:113–117. [PubMed: 14526083]
2. Boillee S, et al. Onset and progression in inherited ALS determined by motor neurons and microglia. *Science*. 2006; 312:1389–1392. [PubMed: 16741123]
3. Yamanaka K, et al. Astrocytes as determinants of disease progression in inherited amyotrophic lateral sclerosis. *Nat Neurosci*. 2008; 11:251–253. [PubMed: 18246065]
4. Ilieva H, Polymenidou M, Cleveland DW. Non-cell autonomous toxicity in neurodegenerative disorders: ALS and beyond. *J Cell Biol*. 2009; 187:761–772. [PubMed: 19951898]
5. Kang SH, Fukaya M, Yang JK, Rothstein JD, Bergles DE. NG2⁺ CNS glial progenitors remain committed to the oligodendrocyte lineage in postnatal life and following neurodegeneration. *Neuron*. 2010; 68:668–681. [PubMed: 21092857]
6. Magnus T, et al. Adult glial precursor proliferation in mutant SOD1G93A mice. *Glia*. 2008; 56:200–208. [PubMed: 18023016]
7. Nave KA. Myelination and support of axonal integrity by glia. *Nature*. 2010; 468:244–252. [PubMed: 21068833]
8. Nave KA, Trapp BD. Axon-glial signaling and the glial support of axon function. *Annu Rev Neurosci*. 2008; 31:535–561. [PubMed: 18558866]
9. Lee Y, et al. Oligodendroglia metabolically support axons and contribute to neurodegeneration. *Nature*. 2012; 487:443–448. [PubMed: 22801498]
10. Suzuki A, et al. Astrocyte-neuron lactate transport is required for long-term memory formation. *Cell*. 2011; 144:810–823. [PubMed: 21376239]
11. Rinholm JE, et al. Regulation of oligodendrocyte development and myelination by glucose and lactate. *J Neurosci*. 2011; 31:538–548. [PubMed: 21228163]

12. Niebroj-Dobosz I, Rafalowska J, Fidzianska A, Gadamski R, Grieb P. Myelin composition of spinal cord in a model of amyotrophic lateral sclerosis (ALS) in SOD1G93A transgenic rats. *Folia Neuropathol.* 2007; 45:236–241. [PubMed: 18176898]
13. Cosottini M, et al. Magnetization transfer imaging demonstrates a distributed pattern of microstructural changes of the cerebral cortex in amyotrophic lateral sclerosis. *AJNR Am J Neuroradiol.* 2011; 32:704–708. [PubMed: 21436337]
14. Rivers LE, et al. PDGFRA/NG2 glia generate myelinating oligodendrocytes and piriform projection neurons in adult mice. *Nat Neurosci.* 2008; 11:1392–1401. [PubMed: 18849983]
15. Zhu X, et al. Age-dependent fate and lineage restriction of single NG2 cells. *Development.* 2011; 138:745–753. [PubMed: 21266410]
16. Gurney ME, et al. Motor neuron degeneration in mice that express a human Cu,Zn superoxide dismutase mutation. *Science.* 1994; 264:1772–1775. [PubMed: 8209258]
17. Dal Canto MC, Gurney ME. Neuropathological changes in two lines of mice carrying a transgene for mutant human Cu,Zn SOD, and in mice overexpressing wild type human SOD: a model of familial amyotrophic lateral sclerosis (FALS). *Brain Res.* 1995; 676:25–40. [PubMed: 7796176]
18. Woodruff RH, Tekki-Kessaris N, Stiles CD, Rowitch DH, Richardson WD. Oligodendrocyte development in the spinal cord and telencephalon: common themes and new perspectives. *Int J Dev Neurosci.* 2001; 19:379–385. [PubMed: 11378298]
19. Guo F, et al. Pyramidal neurons are generated from oligodendroglial progenitor cells in adult piriform cortex. *J Neurosci.* 2010; 30:12036–12049. [PubMed: 20826667]
20. Davalos D, et al. ATP mediates rapid microglial response to local brain injury in vivo. *Nat Neurosci.* 2005; 8:752–758. [PubMed: 15895084]
21. Jamin N, Junier MP, Grannec G, Cadusseau J. Two temporal stages of oligodendroglial response to excitotoxic lesion in the gray matter of the adult rat brain. *Exp Neurol.* 2001; 172:17–28. [PubMed: 11681837]
22. Wu YJ, Tang YF, Xiao ZC, Bao ZM, He BP. NG2 cells response to axonal alteration in the spinal cord white matter in mice with genetic disruption of neurofilament light subunit expression. *Mol Neurodegener.* 2008; 3:18. [PubMed: 18957081]
23. Coutts M, Kong LX, Keirstead HS. A model of motor neuron loss: selective deficits after ricin injection. *J Neurotrauma.* 2010; 27:1333–1342. [PubMed: 20486802]
24. Henson PM, Bratton DL, Fadok VA. Apoptotic cell removal. *Curr Biol.* 2001; 11:R795–805. [PubMed: 11591341]
25. . . .
26. Locatelli G, et al. Primary oligodendrocyte death does not elicit anti-CNS immunity. *Nat Neurosci.* 2012; 15:543–550. [PubMed: 22366759]
27. Pohl HB, et al. Genetically induced adult oligodendrocyte cell death is associated with poor myelin clearance, reduced remyelination, and axonal damage. *J Neurosci.* 2011; 31:1069–1080. [PubMed: 21248132]
28. Woodruff RH, Fruttiger M, Richardson WD, Franklin RJ. Platelet-derived growth factor regulates oligodendrocyte progenitor numbers in adult CNS and their response following CNS demyelination. *Mol Cell Neurosci.* 2004; 25:252–262. [PubMed: 15019942]
29. Chang A, Nishiyama A, Peterson J, Prineas J, Trapp BD. NG2-positive oligodendrocyte progenitor cells in adult human brain and multiple sclerosis lesions. *J Neurosci.* 2000; 20:6404–6412. [PubMed: 10964946]
30. Pouly S, Becher B, Blain M, Antel JP. Expression of a homologue of rat NG2 on human microglia. *Glia.* 1999; 27:259–268. [PubMed: 10457372]
31. Bu J, Akhtar N, Nishiyama A. Transient expression of the NG2 proteoglycan by a subpopulation of activated macrophages in an excitotoxic hippocampal lesion. *Glia.* 2001; 34:296–310. [PubMed: 11360302]
32. Higuchi M, et al. Axonal degeneration induced by targeted expression of mutant human tau in oligodendrocytes of transgenic mice that model glial tauopathies. *J Neurosci.* 2005; 25:9434–9443. [PubMed: 16221853]

33. Yazawa I, et al. Mouse model of multiple system atrophy alpha-synuclein expression in oligodendrocytes causes glial and neuronal degeneration. *Neuron*. 2005; 45:847–859. [PubMed: 15797547]
34. Horner PJ, Thallmair M, Gage FH. Defining the NG2-expressing cell of the adult CNS. *J Neurocytol*. 2002; 31:469–480. [PubMed: 14501217]
35. Funfschilling U, et al. Glycolytic oligodendrocytes maintain myelin and long-term axonal integrity. *Nature*. 2012; 485:517–521. [PubMed: 22622581]
36. Bruijn LI, et al. ALS-linked SOD1 mutant G85R mediates damage to astrocytes and promotes rapidly progressive disease with SOD1-containing inclusions. *Neuron*. 1997; 18:327–338. [PubMed: 9052802]
37. Pramatarova A, Laganier J, Roussel J, Brisebois K, Rouleau GA. Neuron-specific expression of mutant superoxide dismutase 1 in transgenic mice does not lead to motor impairment. *J Neurosci*. 2001; 21:3369–3374. [PubMed: 11331366]
38. Rothstein JD, Van Kammen M, Levey AI, Martin LJ, Kuncl RW. Selective loss of glial glutamate transporter GLT-1 in amyotrophic lateral sclerosis. *Ann Neurol*. 1995; 38:73–84. [PubMed: 7611729]
39. Nagai M, et al. Astrocytes expressing ALS-linked mutated SOD1 release factors selectively toxic to motor neurons. *Nat Neurosci*. 2007; 10:615–622. [PubMed: 17435755]
40. Gong YH, Parsadanian AS, Andreeva A, Snider WD, Elliott JL. Restricted expression of G86R Cu/Zn superoxide dismutase in astrocytes results in astrogliosis but does not cause motoneuron degeneration. *J Neurosci*. 2000; 20:660–665. [PubMed: 10632595]
41. Yamanaka K, et al. Mutant SOD1 in cell types other than motor neurons and oligodendrocytes accelerates onset of disease in ALS mice. *Proc Natl Acad Sci U S A*. 2008; 105:7594–7599. [PubMed: 18492803]
42. Aebischer J, et al. Elevated levels of IFN γ and LIGHT in the spinal cord of patients with sporadic amyotrophic lateral sclerosis. *Eur J Neurol*. 2012; 19:752–759. [PubMed: 22221541]
43. Buntinx M, et al. Cytokine-induced cell death in human oligodendroglial cell lines: I. Synergistic effects of IFN- γ and TNF- α on apoptosis. *J Neurosci Res*. 2004; 76:834–845. [PubMed: 15160395]
44. Neumann M, et al. TDP-43-positive white matter pathology in frontotemporal lobar degeneration with ubiquitin-positive inclusions. *J Neuropathol Exp Neurol*. 2007; 66:177–183. [PubMed: 17356379]
45. Tu PH, et al. Glial cytoplasmic inclusions in white matter oligodendrocytes of multiple system atrophy brains contain insoluble alpha-synuclein. *Ann Neurol*. 1998; 44:415–422. [PubMed: 9749615]
46. Komori T. Tau-positive glial inclusions in progressive supranuclear palsy, corticobasal degeneration and Pick's disease. *Brain Pathol*. 1999; 9:663–679. [PubMed: 10517506]
47. Bauer J, et al. Endoplasmic reticulum stress in PLP-overexpressing transgenic rats: gray matter oligodendrocytes are more vulnerable than white matter oligodendrocytes. *J Neuropathol Exp Neurol*. 2002; 61:12–22. [PubMed: 11829340]
48. Chong SY, et al. Neurite outgrowth inhibitor Nogo-A establishes spatial segregation and extent of oligodendrocyte myelination. *Proc Natl Acad Sci U S A*. 2012; 109:1299–1304. [PubMed: 22160722]
49. Dutta R, Trapp BD. Pathogenesis of axonal and neuronal damage in multiple sclerosis. *Neurology*. 2007; 68:S22–31. discussion S43–54. [PubMed: 17548565]
50. Rudick RA, Trapp BD. Gray-matter injury in multiple sclerosis. *N Engl J Med*. 2009; 361:1505–1506. [PubMed: 19812410]
51. Doerflinger NH, Macklin WB, Popko B. Inducible site-specific recombination in myelinating cells. *Genesis*. 2003; 35:63–72. [PubMed: 12481300]
52. Novak A, Guo C, Yang W, Nagy A, Lobe CG. Z/EG, a double reporter mouse line that expresses enhanced green fluorescent protein upon Cre-mediated excision. *Genesis*. 2000; 28:147–155. [PubMed: 11105057]
53. Srinivas S, et al. Cre reporter strains produced by targeted insertion of EYFP and ECFP into the ROSA26 locus. *BMC Dev Biol*. 2001; 1:4. [PubMed: 11299042]

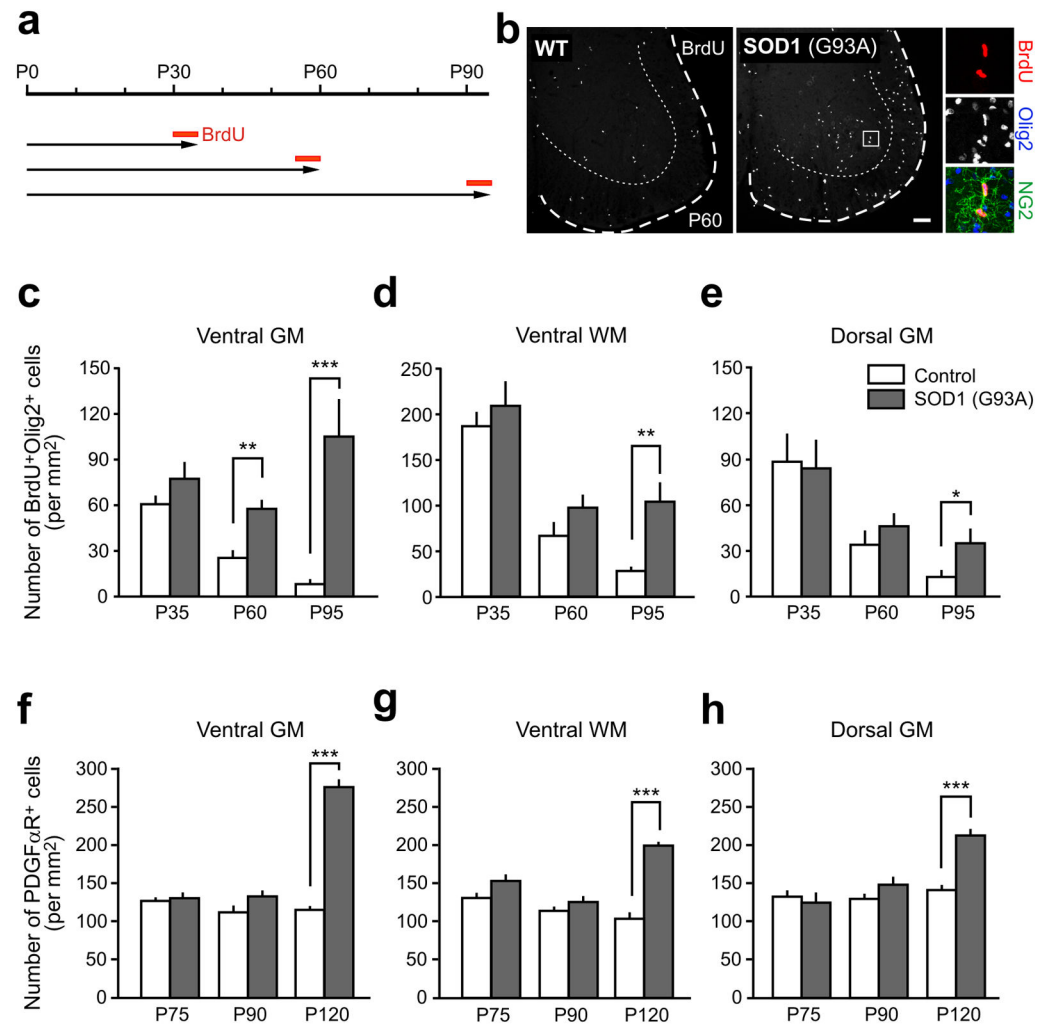
54. Muzumdar MD, Tasic B, Miyamichi K, Li L, Luo L. A global double-fluorescent Cre reporter mouse. *Genesis*. 2007; 45:593–605. [PubMed: 17868096]
55. Gong S, et al. A gene expression atlas of the central nervous system based on bacterial artificial chromosomes. *Nature*. 2003; 425:917–925. [PubMed: 14586460]

Author Manuscript

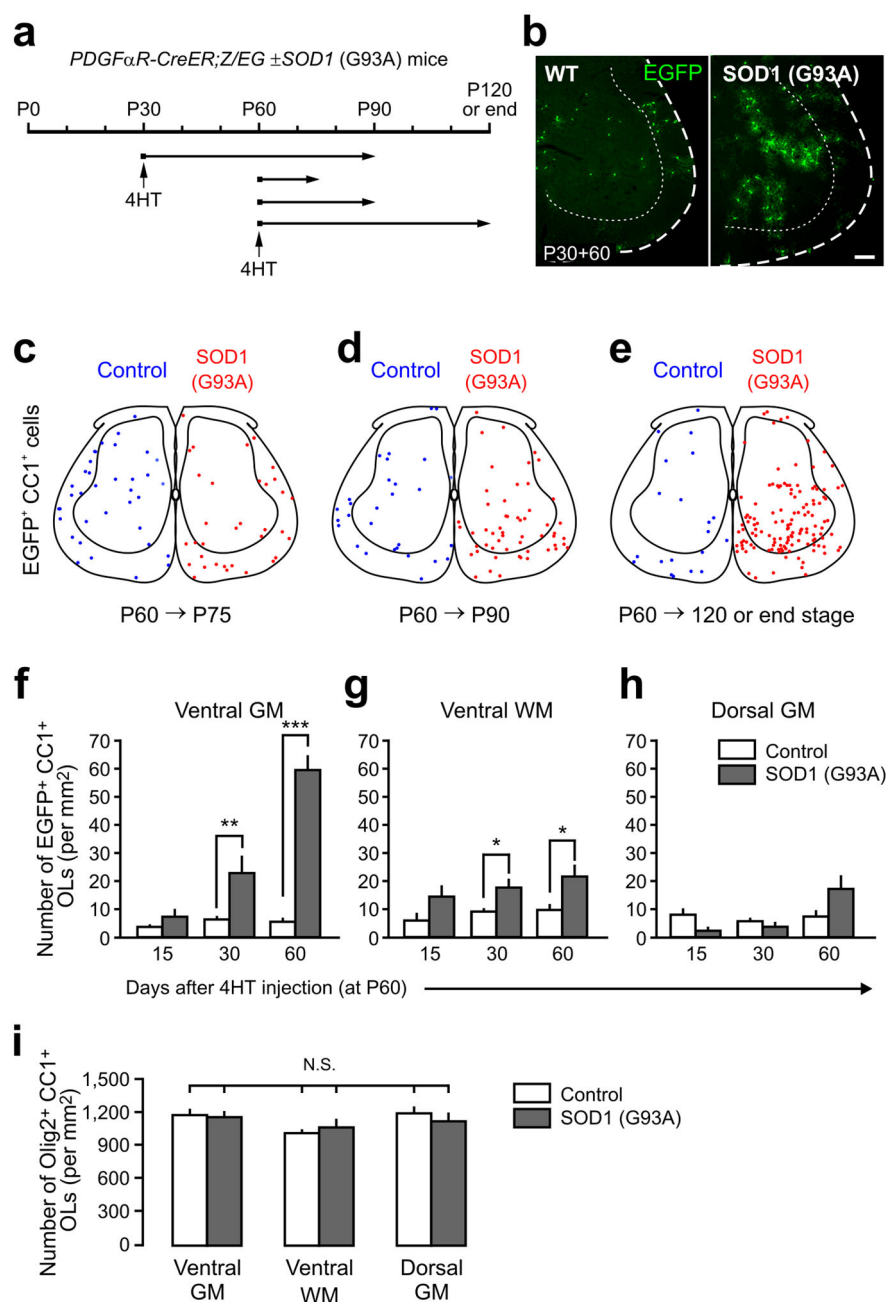
Author Manuscript

Author Manuscript

Author Manuscript

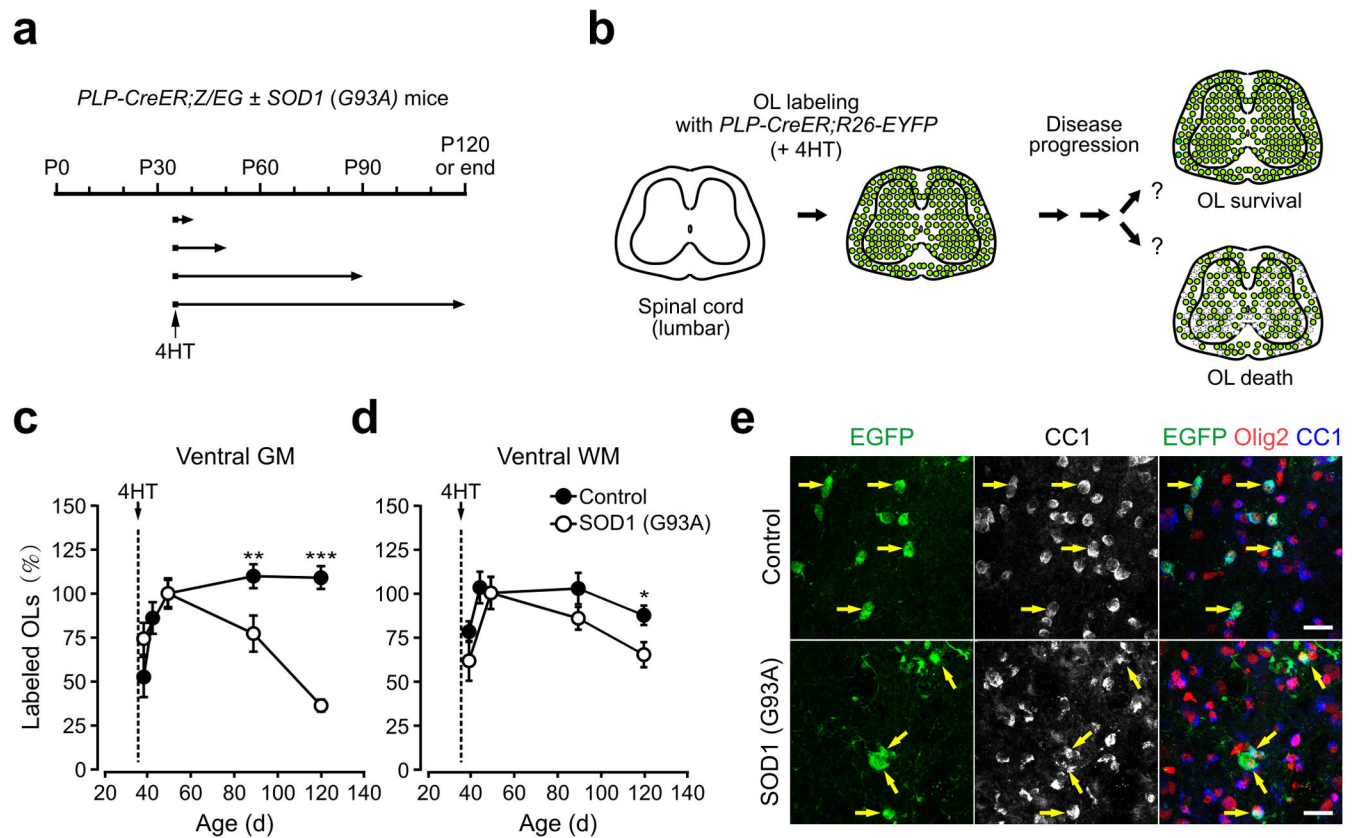
**Figure 1.**

Enhanced proliferation of NG2⁺ cells in the spinal cord of pre-symptomatic ALS mice. (a) BrdU protocol used to assess proliferation of NG2⁺ cells in control and *SOD1* (G93A) mice. (b) Fluorescence images showing BrdU⁺ cells in the ventral horn of the spinal cord in control and *SOD1* (G93A) mice at P60. Panels at right show two BrdU⁺ NG2⁺ cells in the ventral gray matter. Scale bar: 100 μ m. (c – e) Graphs showing the density of proliferating oligodendrocyte lineage cells (BrdU⁺Olig2⁺) in different regions of spinal cord at different ages in control (white bars) and *SOD1* (G93A) (gray bars) mice. (f – h) Graphs showing the density of NG2⁺ cells (PDGF α R⁺) in different regions of the spinal cord at different stages of disease (P75 (pre-symptomatic), P90 (symptomatic), and P120 (end stage)), as compared to wild type mice. GM, gray matter; WM, white matter. Mean + s.e.m. ($n = 9$ sections obtained from 3 mice per group), * $P < 0.05$, ** $P < 0.001$, *** $P < 0.0005$, unpaired Student's t -test.

**Figure 2.**

Enhanced oligodendrogenesis in the spinal cord gray matter of adult ALS mice. **(a)** Protocol used to trace the fate of NG2⁺ cells in *PDGFαR-CreER;Z/EG ± SOD1 (G93A)* mice. Cohorts of NG2⁺ cells were labeled with EGFP by 4HT injection at P30 or P60 then analyzed at different ages. **(b)** Fluorescence images showing EGFP⁺ NG2⁺ cell progeny in the ventral horn of the spinal cord in control or *SOD1 (G93A)* mice 60 days after 4HT administration at P30 (P30+60). Scale bar: 100 μm. **(c – e)** Maps of the location of adult born oligodendrocytes generated from NG2⁺ cells in the spinal cord of control (blue circles) or *SOD1 (G93A)* mice (red circles), from P60 to P75 **(c)**, from P60 to P90 **(d)**, or from P60

to P120 (or end stage for ALS mice) (e). Oligodendrocytes (EGFP⁺CC1⁺) in four randomly sampled lumbar spinal cord sections from each group (from 3–4 mice) are shown. (f – h) Graphs showing the density of newly generated EGFP⁺ CC1⁺ oligodendrocytes in different regions of the adult spinal cord from control (white bars) and *SOD1* (G93A) mice (gray bars). Mean + s.e.m. ($n = 9$ sections from 3 mice per group) * $P < 0.05$, ** $P < 0.001$, *** $P < 0.0005$, unpaired Student's t test. i) Graph showing the overall density of oligodendrocytes (Olig2⁺CC1⁺) in different regions of the spinal cord of P120 and end stage *SOD1* (G93A) mice. Mean + s.e.m. ($n = 12$ sections per group from 4 mice per group) N.S., non-significant, one-way ANOVA with Tukey test.

**Figure 3.**

Progressive degeneration of oligodendrocytes in the spinal cord ventral gray matter of ALS mice. **(a)** Protocol used to track the fate of early-born oligodendrocytes. Littermate control and *SOD1 (G93A)* expressing *PLP-CreER;ROSA26-EYFP* mice received 4HT (2 mg) at P35 and were analyzed at P40, P50, P90 and P120 (or end stage for ALS mice). **(b)** Schematic showing the rationale and possible outcomes of oligodendrocyte fate analysis. **(c,d)** Plot of the number of *EYFP*⁺ oligodendrocytes (*CC1*⁺*Olig2*⁺) in ventral gray matter (GM) **(c)** and ventral white matter (WM) **(d)** of *PLP-CreER;ROSA26-EYFP ± SOD1 (G93A)* mice, expressed relative to the number observed at P35+15 (P50). Note that control group had additional time point (P35+10). Means ± s.e.m. (*n* = 9 sections from 3 mice per each time point of each group). * *P* < 0.05, ** *P* < 0.001, *** *P* < 0.0005. Unpaired Student's *t*-test was used to compare mean values between control and *SOD1 (G93A)* mice at each time point. One-way ANOVA with Tukey test was used for age-dependent relative changes in *EYFP*⁺ oligodendrocytes in each group. **(e)** Confocal images showing the density and morphology of *EYFP*⁺ (stained with anti-EGFP antibody) *CC1*⁺*Olig2*⁺ spinal cord oligodendrocytes (yellow arrows) in ventral gray matter at P120 (control) or at end stage *SOD1 (G93A)* mice. Scale bars: 20μm.

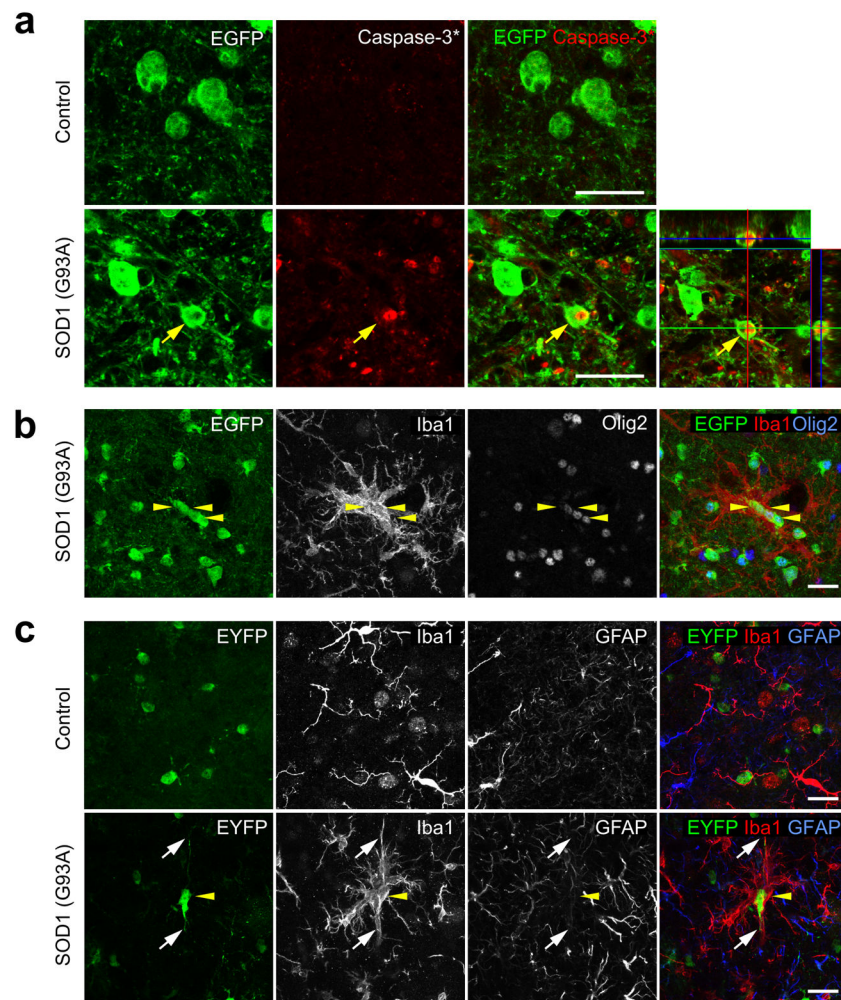


Figure 4.

Apoptosis of oligodendrocytes in the spinal cord of ALS mice. **(a)** Confocal images from the spinal cord ventral gray matter of a *MOBP-EGFP;SOD1 (G93A)* mouse at end stage showing an EGFP⁺ oligodendrocyte (yellow arrow) that was immunopositive for activated caspase-3. Lower right panel is an orthogonal view showing co-localization of activated caspase-3 and EGFP. **(b,c)** Confocal images of the spinal cord ventral gray matter showing Iba1⁺ activated microglia surrounding oligodendrocytes labeled with EGFP **(b)** or EYFP **(c)** in SOD1 (G93A) expressing *MOBP-EGFP* (P90) or *PLP-CreER;ROSA26-EYFP* (P30+60) mice, respectively. Yellow arrowheads highlight several labeled oligodendrocytes, and white arrows in **(c)** highlight the processes of one EYFP⁺ oligodendrocyte. Scale bars: 20 μ m.

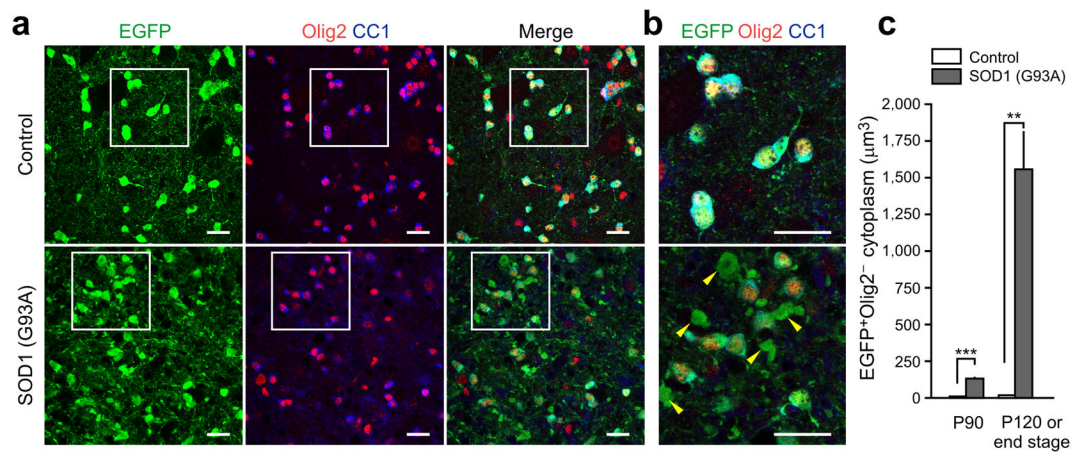


Figure 5.

Early disruption of oligodendrocyte structure in the spinal cord of ALS mice. **(a,b)** Confocal images of EGFP⁺ structures in the ventral spinal cord gray matter from control *MOBP-EGFP* (P120) and *MOBP-EGFP;SOD1 (G93A)* mice (end stage). Panels in **(b)** show regions highlighted by white squares in **(a)**. Arrowheads indicate large EGFP⁺ structures that were Olig2⁻ and CC1⁻. Scale bars: 20 μm. **(c)** Measured volume of Olig2⁻ EGFP⁺ fragments in each 250,000 μm³ imaged volume. Mean + s.e.m. ($n = 6 - 9$ sections from 3 mice per group) ** $P = 1.5 \times 10^{-5}$, *** $P = 8 \times 10^{-6}$, unpaired Student's t -test.

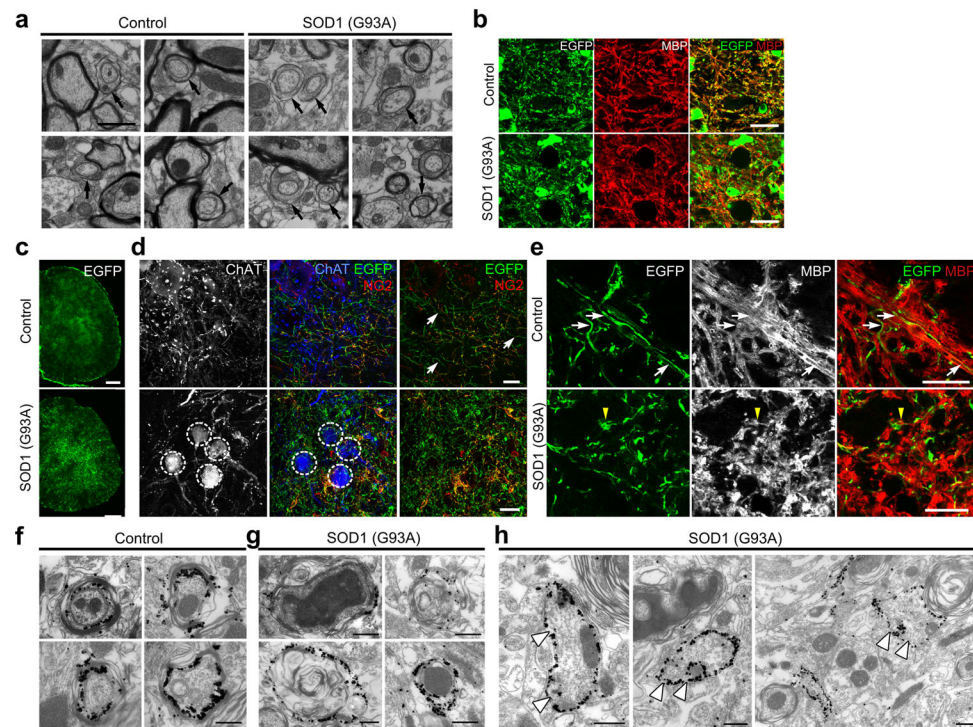


Figure 6.

Myelin abnormalities and impaired maturation of adult-born oligodendrocytes in the spinal cord of ALS mice. **(a)** Electron micrographs of ventral gray matter spinal cord of control (P120) and *SOD1 (G93A)* mice at end stage. Arrows highlight partially myelinated axons. Note the presence of thick oligodendrocyte cytoplasm surrounding these axons. **(b)** Confocal images of MBP immunoreactivity in ventral gray matter of P120 *MOBP-EGFP* mice or end stage *MOBP-EGFP;SOD1 (G93A)* mice. Optical sections: 1.5 μm . **(c)** Fluorescent images of membrane-anchored EGFP in the spinal cord of *PDGF α R-CreER;ROSA26-mEGFP* mice (P60+60). **(d)** Confocal images showing fine EGFP⁺ processes of adult-born oligodendrocytes in ventral gray matter of *PDGF α R-CreER;ROSA26-mEGFP* \pm *SOD1 (G93A)* mice (P60+60). Circles indicate ChAT⁺ motor neuron cell bodies and white arrows indicate NG2⁻ oligodendrocyte processes. **(e)** Confocal images showing co-localization of EGFP⁺ thin processes and MBP immunoreactivity (white arrows) in control *PDGF α R-CreER; ROSA26-mEGFP* mice (P60+60) (upper images). MBP immunoreactivity was more disorganized in *PDGF α R-CreER; ROSA26-mEGFP* mice;*SOD1 (G93A)* mice (lower panel) and rarely co-localized with EGFP⁺ processes (P60+60) (yellow arrowhead). Optical sections: 0.5 μm . **(f–h)** Thin section electron micrographs from *PDGF α R-CreER;ROSA26-mEGFP* \pm *SOD1 (G93A)* mice at P60+60 showing silver-intensified gold labeling of EGFP⁺ oligodendrocyte processes. Large, non-myelinating EGFP⁺ structures (arrowheads) reminiscent of apoptotic bodies were observed frequently in *SOD1 (G93A)* mice **(h)**. Scale bars: 1 μm **(a)**, 20 μm **(b, d, e)**, 200 μm **(c)**, 500 nm **(f–h)**.

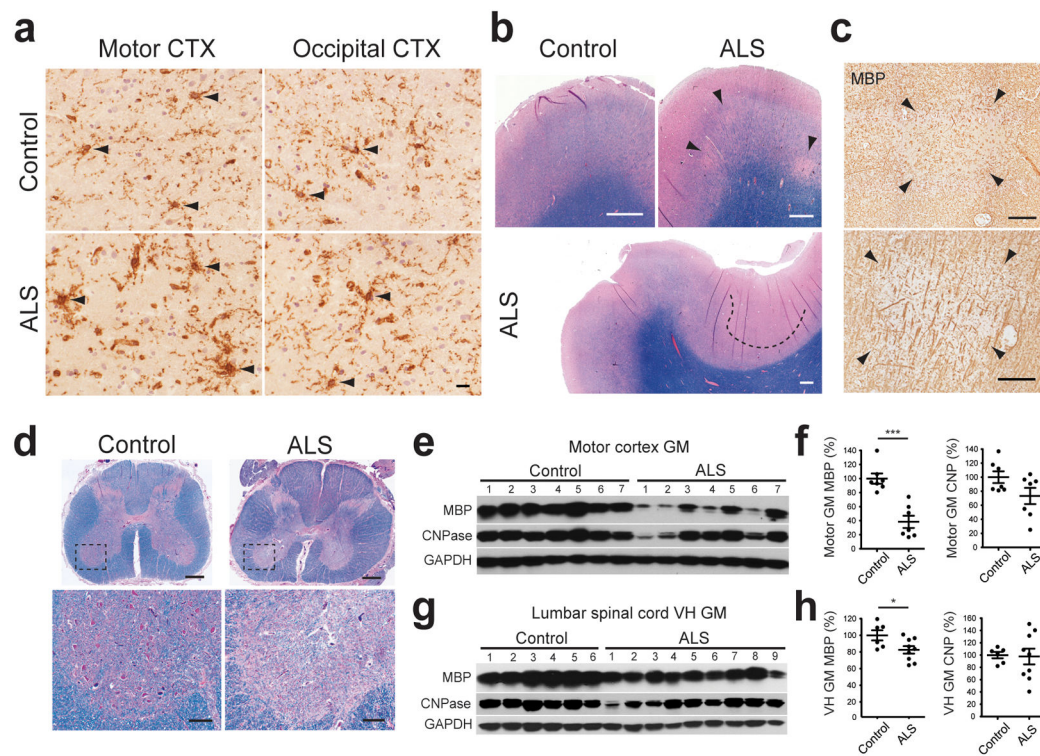


Figure 7.

Demyelination in gray matter regions of the motor cortex and spinal cord in human ALS. **(a)** Sections of motor cortex gray matter from control and ALS patients showing immunoreactivity to NG2. NG2⁺ cells are highlighted by arrowheads. See NG2/Iba1 co-immunostained images in Supplementary Fig. 8a. Images were acquired from cortical layers IV and V. Scale bars: 20 μ m. **(b)** Luxol fast blue staining of motor cortices from control subjects and ALS patients. Demyelinated lesions are highlighted by arrowheads (upper right panel) or a dashed line (lower panel). **(c)** MBP immunoreactivity in ALS motor cortex. Adjacent sections to those shown in the upper right and lower panels in **(b)** were used. Images show demyelinated plaques in layer III (upper panel) and layer V (lower panel). **(d)** Sections of lumbar spinal cord from an ALS patient stained with Luxol fast blue showing demyelination in the ventral horn gray matter and lateral corticospinal tract (arrowhead). Lower panels are higher magnification images of the boxed regions in the upper panels. Scale bars: 1 mm (**b,d** upper panels); 200 μ m (**c,d** lower panels). **(e, g)** Western blots of oligodendrocyte lineage-specific myelin proteins in motor cortex gray matter (**e**) and lumbar spinal cord ventral horn grey matter (**g**) from controls and ALS patients. Full-length blots are presented in Supplementary Fig. 11. **(f, h)** Graphs of MBP and CNPase protein expression levels (measured by Western blot) in the motor cortex (**f**) and lumbar spinal cord ventral horn (**h**) gray matter in controls and ALS patients, normalized to average value in controls. Mean \pm s.e.m. with individual values. * $P < 0.05$, *** $P < 0.0001$, unpaired Student's t -test.

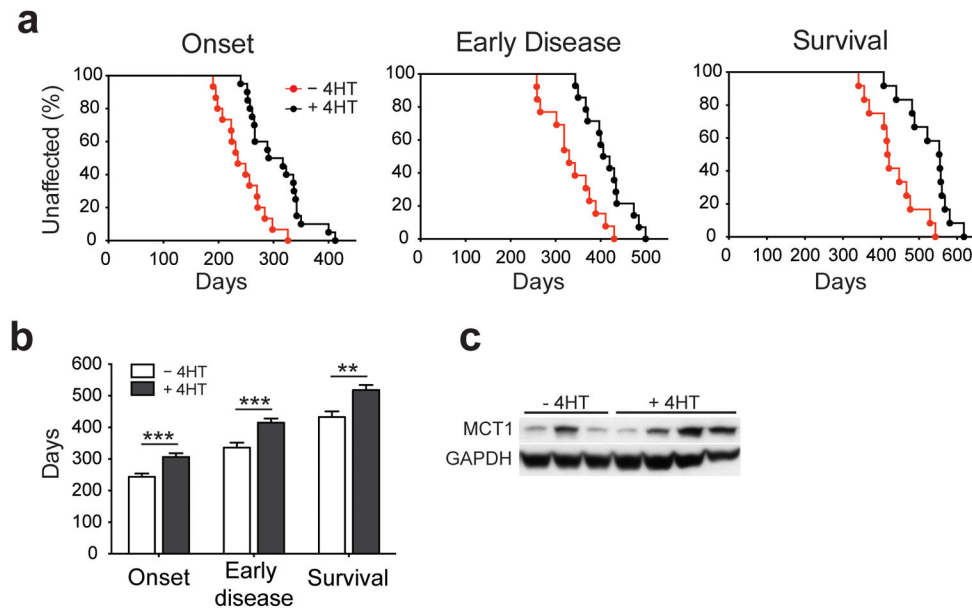


Figure 8.

Excision of mutant SOD1 (G37R) from NG2⁺ cells delays disease onset and prolongs survival in ALS mice. **(a)** Plots of disease onset (median, -4HT: 235 d ($n = 15$); +4HT: 304 d ($n = 20$), $P = 0.0003$, Log-Rank test), early disease (median, -4HT: 330 d ($n = 13$); +4HT: 413 d ($n = 14$), $P = 0.001$), and survival (median, -4HT: 419 d ($n = 12$); +4HT: 554 d ($n = 14$), $P = 0.0005$) of *PDGFR-CreER;loxSOD1 (G37R)* mice. **(b)** Comparison of mean age at disease onset (-4HT: 244 ± 10 d; +4HT: 307 ± 11 d, $P = 0.0005$), early disease (-4HT: 336 ± 16 d; +4HT: 415 ± 13 d, $P = 0.001$) and survival (-4HT: 433 ± 18 d; +4HT: 518 ± 16 d, $P = 0.0025$). Mean + s.e.m. ** $P < 0.01$; *** $P < 0.005$, Mann Whitney test. **(c)** Western blots of MCT1 expression from several -4HT and +4HT mice examined at disease onset. Full-length blots are presented in Supplementary Fig. 11.